# Parotid Gland Tissues Investigated by Picosecond Time-Gated and Optical Spectroscopic Imaging Techniques

S. K. Gayen, Mohammad Alrubaiee, Howard E. Savage, Stimson P. Schantz, and R. R. Alfano, *Fellow, IEEE*

***Abstract*—Near-infrared (NIR) time-resolved and spectroscopic transillumination imaging techniques are used to investigate normal tissues and Warthin's tumor of human parotid glands. The time-sliced imaging arrangement uses 120-fs, 1-kHz repetition-rate, 800-nm pulses from a Ti : sapphire laser and amplifier system for sample illumination and an ultrafast gated intensified camera system (UGICS) for recording two-dimensional (2-D) images using transmitted light. Images recorded with earlier temporal slices (approximately first 100 ps) of transmitted light highlight the tumor, while those recorded with later temporal slices (later than 200 ps) accentuate normal tissues. The spectroscopic imaging arrangement uses 1210–1300 nm tunable output of a Cr : forsterite laser for sample illumination, a Fourier space gate to discriminate against multiple-scattered light, and a NIR area camera to record 2-D images. The tumor region in the specimen appears brighter than the normal region in spectroscopic images recorded with light of different wavelengths. A wavelength-dependent variation in the ratio of light transmission through the tumor to that through the normal parotid gland is observed. Differences in scattering and wavelength-dependent absorption characteristics of normal parotid gland and Warthin's tumor provide a consistent explanation of these observed features. Histopathological analysis of the specimen sheds light on the probable origin of the differences in scattering and absorption characteristics.**

***Index Terms*—Near-infrared imaging, optical biomedical imaging, parotid gland, photon propagation in highly scattering media, time-gated imaging, transillumination imaging, Warthin's tumor.**

## I. Introduction

OPTICAL biomedical imaging techniques are attracting interest as promising noninvasive means for detection and diagnosis of tumors and abnormalities in human body [1]–[11]. Body organs that are potentially amenable to optical imaging investigation include breast, brain, gastro-intestinal tract, obstetric and gynecological tract, prostate, skin, salivary glands, arteries, and bones. Development of appropriate and effective optical modalities for *in vivo* clinical imaging of lesions in any of these organs is an involved process. An important step in this development process is testing of the efficacy of the method on *ex vivo* tissue specimens of the target organ, which in turn provides key information about light transport and optical spectroscopic characteristics of the types of tissues under investigation. We have initiated such a study of *ex vivo* normal and abnormal tissues from different organs using a variety of near-infrared (NIR) optical imaging techniques. In this paper, we present results of time-sliced and spectroscopic two-dimensional (2-D) NIR imaging experiments on excised normal tissues and Warthin's tumor of the parotid gland.

Time-sliced imaging [6], [10], [12] is an extension of the concept of time-resolved early-light imaging [13]–[17] wherein a sequence of 2-D images of the sample under investigation is recorded using different temporal slices of light emergent from the sample, in addition to the early-arriving part. Differences in light transport properties of constituent tissues in a sample are highlighted in the 2-D images obtained with different temporal slices of the transmitted light. We use ultrashort pulses of light from a femtosecond Ti:sapphire laser to illuminate the sample and a time-gated camera with a variable gate position to record 2-D images with the gated fraction of the forward transmitted light.

Spectroscopic imaging [18] uses light of different colors to exploit any spectroscopic difference for enhancing image contrast and exploring diagnostic potential. In a spectroscopic imaging measurement, one uses light of different wavelengths to record 2-D transillumination images of the sample under investigation. If a part of the sample happens to have a different response to light at a particular wavelength than the rest, then "resonant" (or "near-resonant") images recorded with light of that wavelength (or a wavelength near the resonance) provide contrast between that part and rest of the sample [18]. Comparisons with "nonresonant" images that are obtained using light of wavelengths away from the resonance help accentuate the contrast even further.

The parotid glands, located in the tissue inferior and anterior to the ears, are the largest of the three main pairs of salivary glands [19]. They secrete the serous (thin, watery) component of the saliva, and the parotid duct delivers the secretion into the mouth. Diseases of the parotid glands include Warthin's tumor (*cystadenoma lymphomatosum*) [20], and pleomorphic adenoma. In this article, we present results of optical imaging experiments on an *ex vivo* tissue specimen with normal parotid gland tissue and Warthin's tumor. Warthin's tumor is the second most common benign tumor that accounts for 5% to 10% of

Manuscript received April 9, 2001. This work was supported in part by US-AMRMC, DOE, and the NASA IRA Program.

S. K. Gayen, M. Alrubaiee, and R. R. Alfano are with the Institute for Ultrafast Spectroscopy and Lasers, New York State Center for Advanced Technology for Ultrafast Photonic Materials and Applications, Department of Physics, The City College of the City University New York, New York, NY 10031 USA.

H. E. Savage and S. P. Schantz are with the New York Eye and Ear Infirmary, New York, NY 10003 USA and also with Strang Cancer Prevention Center, New York, NY 10021 USA.

Publisher Item Identifier S 1077-260X(01)11189-5.

all parotid gland tumors. The tumor commonly is a round to oval encapsulated mass 1 cm to 10 cm in diameter with a characteristic lymphoid component. It is located in the parotid or preparotid lymph nodes in 99% of the cases [21], [22]. The cut surface of the tumor is gray in color and has cystic or cleftlike spaces filled with a gray or light brown mucinous secretion. Tall columnar cells that overlie lymphoid tissue line the cystic or cleft like spaces.

The remainder of the article is organized as follows. Section II presents an outline of the experimental methods, and a brief description of the samples used in the experiment. Section III presents optical imaging results along with histopathological analysis of the samples. In Section IV, we discuss the implications of the experimental results.

## II. Experimental Methods

### A. Time-Sliced Imaging

Experimental arrangement for time-sliced imaging, shown schematically in Fig. 1(a), made use of approximately 120-fs duration, 1-kHz repetition-rate pulses from a Ti : sapphire laser and amplifier system [23] for sample illumination, and an ultrafast gated intensified camera system (UGICS) for recording 2-D images using picosecond-duration slices of light transmitted through the sample. The laser output was tunable over the 750–850 nm spectral range with an average power of 3 W. We used approximately 200 mW at 800 nm for experiments reported here. A beam expander expanded the beam and an aperture selected a 3-cm diameter central part of it to illuminate the sample.

The UGICS was a compact time-gated image intensifier unit that was fiber-optically coupled to a charge-coupled device (CCD) camera. It provided an electronic time gate whose FWHM duration could be adjusted to a minimum of approximately 80 ps. The temporal position of the gate could be electronically varied over a 20-ns range with a minimum step size of 25 ps. The CCD camera had a 384 × 286 pixels sensing element with a pixel size of 23 $\mu$m × 23 $\mu$m. A 24-mm focal-length $f/2.8$ camera lens collected the signal transmitted through the tissue sample and directed it to the sensing element. The transillumination signal recorded by the UGICS at a particular gate position was a convolution of the transmitted light pulse with the gate pulse centered on the gate position. A personal computer stored and displayed the resulting 2-D images.

### B. Spectroscopic Imaging

The experimental arrangement for near-infrared (NIR) spectroscopic imaging, displayed in Fig. 1(b), used the 1210–1300 nm continuous-wave mode-locked output of a $Cr^{4+}$ : forsterite laser to illuminate the sample. A set of calibrated neutral density filters helped maintain the average optical power of the incident beam at approximately 35 mW for all the wavelengths used in the imaging experiment. A beam expander expanded the beam and an aperture selected a 3-cm diameter central part of it to illuminate the sample.

A Fourier space gate [24] selected out a fraction of the less-scattered image-bearing photons from the strong background

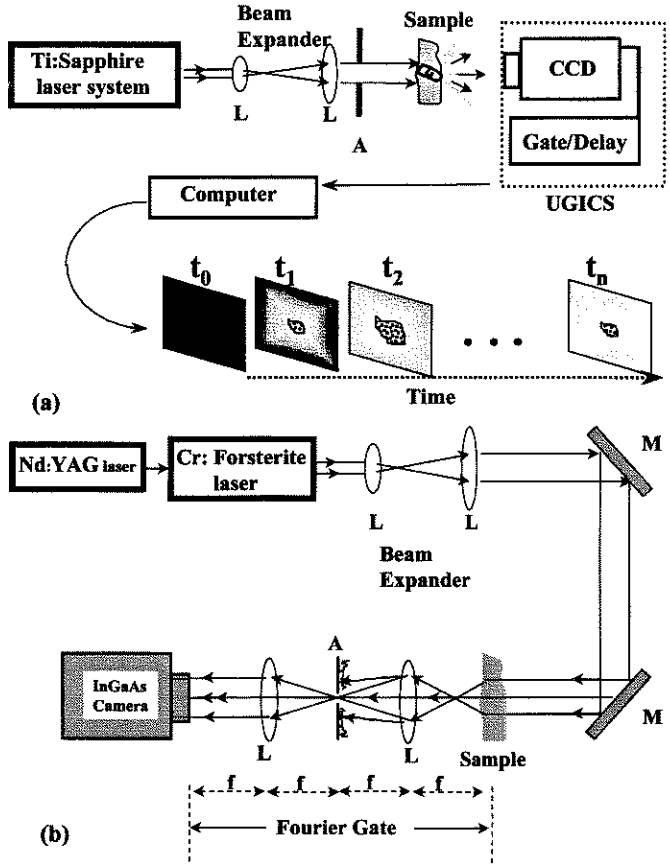


Fig. 1. Schematic diagram of the experimental arrangement for: (a) time-sliced imaging and (b) spectroscopic imaging. Key: A = aperture, L = lens, M = mirror, CCD = charge-coupled device, UGICS = ultrafast gated intensified camera system.

of the image-blurring diffuse photons. A 50 mm focal-length camera lens placed on the optical axis at a distance of 50 mm from the aperture in the Fourier gate collected and collimated the low-spatial-frequency light filtered by the aperture and directed it to the 128 × 128 pixels sensing element of an InGaAs near-infrared (NIR) area camera.

### C. Sample

Excised parotid gland tissue specimen used in the experiments reported in this article was obtained from the New York Eye and Ear Infirmary (NYEEI) under Internal Review Board approvals at the City College of New York and NYEEI. The specimen came from the left parotid gland of a 37-year-old male patient. It was a gray/brown nodule surrounded by normal salivary gland parenchyma. The nodule itself was focally cystic with a papillary appearance. The clinical diagnosis was a benign Warthin's tumor of the left parotid gland.

The specimen was received on ice. It was held between two glass plates and slightly compressed to ensure same overall thickness for optical imaging measurements. The dimensions of this slightly compressed sample were 20 mm × 10 mm × 5 mm. Light transited through the 5 mm path length of the sample for transillumination imaging measurements reported here. After NIR imaging experiments, the sample was placed in formalin and transferred to NYEEI for histological analysis.

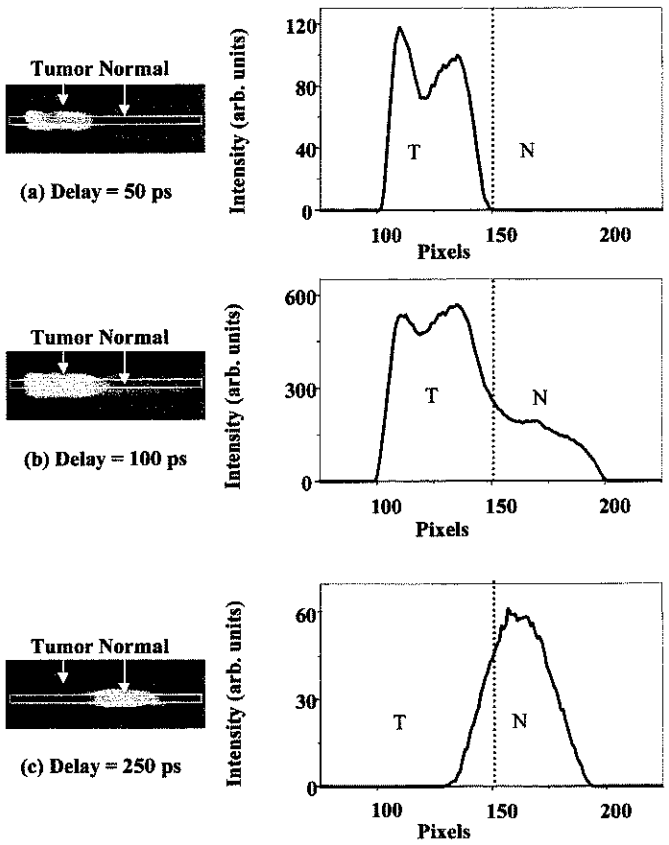


Fig. 2. Time-sliced 2-D images (left frames) of a 20 mm × 10 mm × 5 mm parotid gland tissue sample with normal parotid gland (N) and Warthin's tumor (T) for gate positions of (a) 50 ps, (b) 100 ps, and (c) 250 ps. Corresponding spatial intensity profiles integrated over the same horizontal area highlighted by white dashed boxes in the images are shown in the right side frames. The zero position was taken to be the time of arrival of the light pulse through a 5-mm-thick quartz cell filled with water.

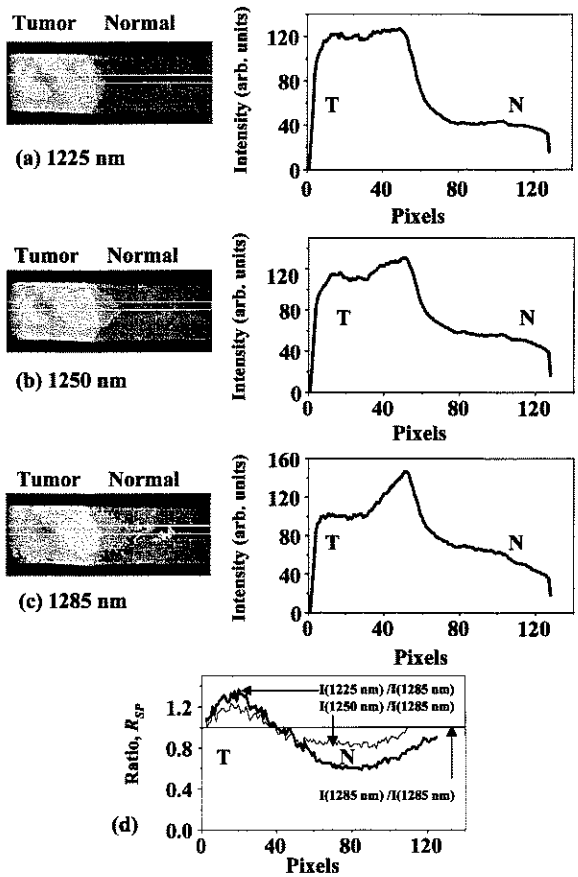


Fig. 3. Spectroscopic 2-D images (left frames) of the parotid gland tissue sample with normal parotid gland (N) and Warthin's tumor (T) for light of wavelengths (a) 1225 nm, (b) 1250 nm, and (c) 1285 nm. Corresponding spatial intensity profiles integrated over the same horizontal area highlighted by white dashed boxes in the images are shown in the right frames. No time gating was used. (d) Spatial profiles of the ratio of intensities $R_{SP}(\lambda)$, as described in the text, for the reference wavelength of 1285 nm, and probing wavelengths of 1225 and 1250 nm.

## III. Results

### A. Time-Sliced Imaging

Time-sliced 2-D transillumination images of the parotid gland sample for gate positions of 50 ps, 100 ps, and 250 ps are displayed in the left frames of Fig. 2(a)–(c), respectively. The zero position was taken to be the time of arrival of the light pulse through a 5-mm-thick quartz cell filled with water. The corresponding frames to the right present the spatial intensity profiles of the respective images integrated over the same horizontal area in all the figures. The salient feature of the images is the differences in time-dependent brightness of the normal tissue and Warthin's tumor in the sample. In the early 50-ps image of Fig. 2(a) only the tumor is visible. The corresponding horizontal spatial profile exhibits peak in the tumor region and hits the baseline in the normal tissue region. At this early time, markedly more light is transmitted through the tumor than the normal parotid gland tissue. With time the image of normal parotid gland tissue gains in brightness and the corresponding region of the spatial profile rises above the baseline, as the typical sampling of Fig. 2(b) for the delay position of 100 ps shows. At later times (250 ps) the image of the normal gland becomes brighter than the tumor, the corresponding spatial profile peaks in the normal gland position indicating higher light transmission through the normal gland than the tumor [Fig. 2(c)].

These results indicate that light transits faster through Warthin's tumor than normal parotid gland tissue. Lower scattering or/and higher absorption of light by the tumor may account for the observed temporal behavior. Since there is no known absorption of 800-nm light by parotid gland tissues, we attribute these time-dependent differences in the relative light transmission through Warthin's tumor and normal parotid gland tissues to the differences in the light scattering characteristics of these components of tissues.

### B. Spectroscopic Imaging

Spectroscopic images of the specimen recorded using light of wavelengths 1225, 1250, and 1285 nm appear in the left side frames of Fig. 3(a)–(c), respectively. Corresponding spatial profiles integrated over the same horizontal area in all the images appear in the right side frames. The salient feature of the images is the higher brightness of the Warthin's tumor region compared to the normal parotid gland region for all three wavelengths.

Since no time gating is used in spectroscopic imaging, the result is indicative of higher overall light transmission through the tumor than that through the normal parotid gland.

Another subtle feature is the wavelength dependence of relative light transmission through the tumor and the normal tissue. We examined the variation in relative brightness with wavelength by monitoring the tumor-to-normal intensity ratio, $R_{\mathrm{TN}}(\lambda) = I_{\mathrm{tumor}}(\lambda)/I_{\mathrm{normal}}(\lambda)$, where $I_{\mathrm{tumor}}(\lambda)$ and $I_{\mathrm{normal}}(\lambda)$, are the averaged intensities through the Warthin's tumor and normal parotid gland regions, respectively, of the spatial profile at wavelength $\lambda$. The values of $R_{\mathrm{TN}}(\lambda)$ for 1225, 1250, and 1285 nm are 2.9, 2.0, and 1.7, respectively.

Even more instructive is the ratio of intensities $R_{\mathrm{SP}}(\lambda) = I(\lambda)/I(\lambda_{\mathrm{R}})$, where $I(\lambda)$ and $I(\lambda_{\mathrm{R}})$, are the values of intensities at probing wavelength $\lambda$ and selected reference wavelength $\lambda_{\mathrm{R}}$, respectively, measured at the same location in the respective images. The horizontal spatial profiles of $R_{\mathrm{SP}}(\lambda)$ for $\lambda_{\mathrm{R}} = 1285$ nm and $\lambda = 1225$ and 1250 nm averaged over the width of the dashed lines in the images of Fig. 3(a)–(c) are shown in Fig. 3(d). These profiles were obtained by taking the ratio of spatial profile at wavelength $\lambda$ to that at 1285 nm. The salient feature of the $R_{\mathrm{SP}}(\lambda)$ profiles in Fig. 3(d) is that the tumor region tends to have a higher value of the ratio ($>1$) than the normal region ($<1$).

The transition region between the Warthin's tumor and normal parotid gland appears brighter than the rest of the tumor in the spectroscopic images and the corresponding spatial intensity profiles tend to peak around pixel 50. The peak is more prominent in the spatial profile of Fig. 3(c) than in other profiles. A histological examination of the specimen revealed that although this region was composed of the same lymphoid and epithelial elements as the rest of the tumor, the tissue in this area was less dense and had more lymphoid tissue than epithelial tissue compared to the rest of the tumor. These differences lead to higher light transmission through the transition region. This result indicates the sensitivity of spectroscopic imaging to variations in tissue density and morphology.

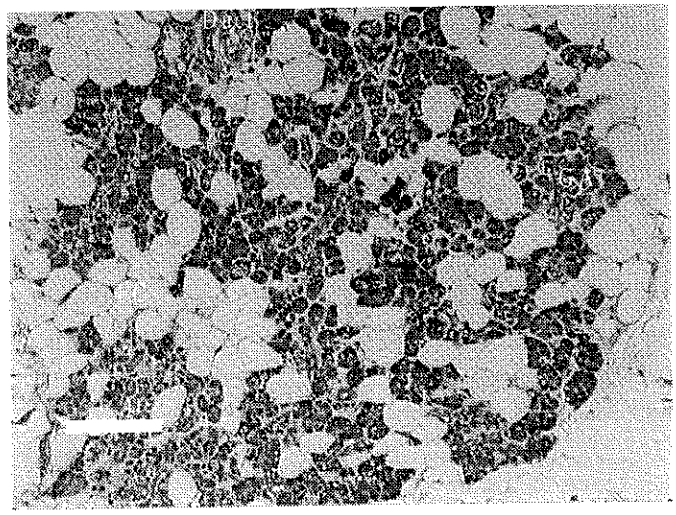

(a)

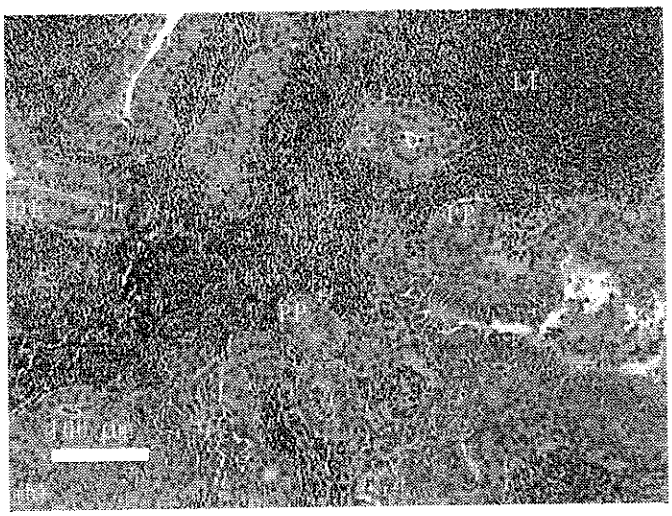

(b)

Fig. 4. Histological micrograph of a representative section from: (a) the normal parotid gland used in the optical imaging experiment showing fat cells (FC), glandular alveoli (GA), and ducts (Duct) and (b) the Warthin's tumor showing double layers (columnar and cuboidal) of ductal epithelium (DE), clefts of the duct (CD), papillary projections (PP) of the ductal epithelium, cystic spaces (CS), and areas of lymphoid tissue (LT).

## IV. Discussion

The results of both the time-sliced imaging and spectroscopic imaging experiments show the ability of the two techniques to select between the Warthin's tumor and normal parotid gland tissues. The contrast between the Warthin's tumor and the normal parotid gland is most dramatic in the images recorded with earlier and later time slices. We observed similar contrast between normal and cancerous regions in the time-sliced images of human breast tissue specimens as well [6], [25].

Spectroscopic images exhibit three main features: (a) overall higher light transmission through the tumor; (b) a wavelength-dependent variation in tumor-to-normal intensity ratio, $R_{\mathrm{TN}}(\lambda)$; and (c) a variation in the spatial profile of the ratio, $R_{\mathrm{SP}}(\lambda)$ between the tumor and normal regions of a specimen. We attribute the higher light transmission through the Warthin's tumor compared to that through the normal parotid gland at all three wavelengths to lower light scattering by the tumor. This attribution is consistent with the results of the time-sliced imaging experiment carried out with 800-nm femtosecond light pulses. The wavelength dependent variation in $R_{\mathrm{TN}}(\lambda)$ and $R_{\mathrm{SP}}(\lambda)$ is expected to be associated with difference in absorption by the normal parotid gland and tumor.

In order to obtain a better appreciation of the origin of the differences in scattering and absorption characteristics of normal parotid gland and Warthin's tumor, we turned to the histopathological analysis of the sample. Histopathology provides detailed information about the structural differences between the normal and abnormal tissues and sets the standard against which the performance of any new technique should be evaluated.

Fig. 4(a) presents a histological micrograph of a representative section of the normal parotid gland tissue used in the optical imaging experiment. The key features are the fat cells (FC), glandular alveoli (GA), and ducts (Duct). Fig. 4(b) is a micrograph of a similar representative section from the Warthin's tumor in the specimen under same magnification. The features in the histology of the Warthin's tumor are double layers (columnar and cuboidal) of ductal epithelium (DE),

clefts of the duct (CD), papillary projections (PP) of the ductal epithelium, cystic spaces (CS), and areas of lymphoid tissue (LT). The contrast with the histology of the normal parotid gland is quite distinct.

Light scattering depends on the size, shape, and relative refractive indices of the scattering entities. The aforementioned structural differences between the tumor and normal parotid gland are likely to lead to different light scattering and spectroscopic characteristics. A quantitative evaluation of the role of different scatterers is highly involved that will require independent measurement of the optical and scattering characteristics of each of the different scattering entities, and modeling of their distribution in the tissue ultrastructure.

A particularly significant difference observed in the micrographs of the two representative sections that has important consequences for NIR imaging experiments is the paucity of fat (adipose) cells in the Warthin's tumor, and their abundance in the normal parotid gland. Two characteristics of adipose tissues may shed light on the observed results of NIR imaging experiments. First, adipose tissues scatter light more effectively than other types of tissues, such as, fibrous, glandular, and ductal [6], [25], [26]. Second, adipose tissue has a broad optical absorption band centered on 1203 nm [26]. The histological analysis shows that the normal parotid gland tissue has a much higher abundance of adipose cells than that in Warthin's tumor. Light transiting through the normal tissue will be more scattered by the adipose cells, traverse longer distance within the sample, and arrive later in time than that transiting through the Warthin's tumor. It thus provides an explanation of the results of time-sliced imaging experiments that show early-light images highlighting the tumor, while the late-light images accentuate the normal parotid gland.

The results of spectroscopic imaging arrangement may be explained as well. The normal part of the sample appears darker in the spectroscopic images Fig. 3(a)–(c) as the more abundant adipose cells there contribute to higher scattering (more loss of light) than the tissues in the tumor. Adipose cells in the normal parotid gland are one of the major contributors to the scattering, but may not be the sole reason for higher scattering by normal tissue.

The light wavelength of 1225 nm is closer to the adipose absorption peak at 1203 nm, 1250 nm is in the wing of the absorption band, while 1285 nm is away from the absorption resonance. Consequently, among the three wavelengths presented in Fig. 3(a)–(c), 1225-nm light is absorbed the most by the adipose cells in the normal part of the specimen, 1285-nm light the least, with the 1250-nm light in between. This wavelength-dependent absorption contributes to the observed decrease in the ratio between 1225 nm to 1285 nm. The tumor-to-normal ratio $R_{\mathrm{TN}}(\lambda)$ thus acts as a parameter to differentiate between normal tissue and Warthin's tumor of the parotid gland. The use of this ratio for *in vivo* application requires knowledge of the suspect region and a normal region, and evaluation of the ratio between transmitted intensities through the abnormal to normal region.

The ratio $R_{\mathrm{SP}}(\lambda)$ is a more promising parameter since it involves measurements of two intensities, one at a reference wavelength and the other at a wavelength near-resonant with adipose absorption, at the same location and evaluation of the ratio. In obtaining the spatial profiles of $R_{\mathrm{SP}}(\lambda)$ displayed in Fig. 3(d), we used 1285 nm that is far-removed from the adipose resonance peak at 1203 nm as the reference wavelength, and 1225 and 1250 nm that lie within the adipose optical absorption band as probing wavelengths. We obtain a higher contrast between the tumor and normal regions in the $R_{\mathrm{SP}}(\lambda)$ profile that uses intensities at 1225 nm, the wavelength closer to the resonance peak. However, in both the $R_{\mathrm{SP}}(\lambda)$ profiles using 1225 nm and 1250 nm, the ratio values tend to be more than one for the tumor region, and less than 1 for the normal region. Assuming that this trend holds, a measurement of $R_{\mathrm{SP}}(\lambda)$ value at a location in the specimen may identify it as either tumor ($R_{\mathrm{SP}} > 1$) or normal ($R_{\mathrm{SP}} < 1$), and no comparison with another region is needed. More measurements on a larger number of samples with different stages of tumor progression will be needed to build up statistics for establishing the values of parameters $R_{\mathrm{SP}}$ and $R_{\mathrm{TN}}$ that will be indicative of the status of tissue (tumor or normal) with requisite specificity.

In summary, the results of these experiments further demonstrate the potential of NIR time-sliced and spectroscopic imaging techniques for detection and diagnosis of tumors in optically accessible suspect body organs.

## ACKNOWLEDGMENT

The authors acknowledge M. Zevallos, A. Katz, and J. Evans for technical help, and S. McCormick for a helpful discussion.

## REFERENCES

[1] G. J. Muller, R. R. Alfano, S. R. Arridge, J. Beuthan, E. Gratton, M. Kaschke, B. R. Masters, S. Svanberg, and P. van der Zeect, Eds., *Medical Optical Tomography: Functional Imaging and Monitoring*. ser. SPIE Institute Series. Bellingham, WA: SPIE, 1993, vol. IS 11.

[2] S. K. Gayen and R. R. Alfano, "Emerging optical biomedical imaging techniques," *Opt. Photon. News*, vol. 7, no. 3, pp. 17–22, 1996.

[3] D. Grosenick, H. Wabnitz, H. Rinneberg, K. T. Moesta, and P. Schlag, "Development of a time-domain optical mammography system and first *in vivo* applications," *Appl. Opt.*, vol. 38, pp. 2927–2943, 1999.

[4] M. A. Francheschini, K. T. Moesta, S. Fantini, G. Gaida, E. Gratton, H. Hess, W. W. Mantulin, M. Seeber, P. M. Schlag, and M. Kaschke, "Frequency-domain techniques enhance optical mammography: Initial clinical results," *Proc. Nal. Acad. Sci. USA*, vol. 94, pp. 6468–6473, 1997.

[5] S. A. Boppart, B. E. Bouma, C. Pitris, J. F. Southern, M. E. Brezinski, and J. G. Fujimoto, "*In vivo* cellular optical coherence tomography imaging," *Nature Med.*, vol. 4, pp. 861–864, 1998.

[6] S. K. Gayen and R. R. Alfano, "Sensing lesions in tissues with light," *Opt. Express*, vol. 4, pp. 475–480, 1999.

[7] J. C. Hebden, S. R. Arridge, and D. T. Deply, "Optical imaging in medicine: I. Experimental techniques," *Phys. Med. Biol.*, vol. 42, pp. 841–853, 1997.

[8] B. Chance, M. Cope, E. Gratton, N. Ramanujam, and B. Tromberg, "Phase measurement of light absorption and scatter in human tissues," *Rev. Sci. Instrum.*, vol. 69, pp. 3457–3481, 1998.

[9] T. O. McBride, B. W. Pogue, E. Gerety, S. Poplack, U. L. Osterberg, and K. D. Paulsen, "Spectroscopic diffuse optical tomography for quantitatively assessing hemoglobin concentration and oxygenation in tissue," *Appl. Opt.*, vol. 38, pp. 5480–5490, 1999.

[10] M. E. Zevallos, S. K. Gayen, B. B. Das, M. Alrubaiee, and R. R. Alfano, "Picosecond electronic time-gated imaging of bones in tissues," *IEEE J. Select. Topics Quantum Electron.*, vol. 5, pp. 916–922, July/Aug. 1999.

[11] H. Eda, I. Oda, Y. Ito, Y. Wada, Y. Oikawa, Y. Tsunazawa, M. Takada, Y. Tsuchiya, Y. Yamashita, A. Sassarolli, Y. Yamada, and M. Tamura, "Multichannel time-resolved tomographic imaging system," *Rev. Sci. Instrum.*, vol. 70, pp. 3593–3602, 1999.

[12] W. Cai, S. K. Gayen, M. Xu, M. Zevallos, M. Alrubaiee, M. Lax, and R. R. Alfano, "Optical tomographic image reconstruction from ultrafast time-sliced transmission measurements," *Appl. Opt.*, vol. 38, pp. 4237–4246, 1999.

[13] K. M. Yoo and R. R. Alfano, "Time-resolved coherent and incoherent components of forward light scattering in random media," *Opt. Lett.*, vol. 15, pp. 320–322, 1990.
[14] R. R. Alfano, X. Linag, L. Wang, and P. Ho, "Time-resolved imaging of translucent dropets in highly scattering media," *Science*, vol. 264, pp. 1913–1915, 1994.
[15] L. Wang, P. P. Ho, G. Liu, G. Zhang, and R. R. Alfano, "Ballistic 2-D imaging through scattering walls using an ultrafast optical Kerr Gate," *Science*, vol. 253, pp. 769–771, 1991.
[16] M. S. Patterson, B. Chance, and B. C. Wilson, "Time-resolved reflectance and transmittance for the noninvasive measurement of tissue optical properties," *Appl. Opt.*, vol. 28, pp. 2331–2336, 1989.
[17] B. B. Das, K. M. Yoo, and R. R. Alfano, "Ultrafast time gated imaging in thick tissues: A step toward optical mammography," *Opt. Lett.*, vol. 18, pp. 1092–1094, 1993.
[18] S. K. Gayen, M. E. Zevallos, M. Alrubaiee, and R. R. Alfano, "Near-infrared laser spectroscopic imaging: A step toward diagnostic optical imaging of human tissues," *Laser Life Sci.*, vol. 8, pp. 187–198, 1999.
[19] E. P. Solomon and P. W. Davis, *Human Anatomy and Physiology*. Philadelphia, PA: CBS, 1983.
[20] A. S. Warthin, "Papillary cystadenoma lymphomatosum," *J. Cancer Res.*, vol. 13, pp. 116–125, 1929.
[21] J. W. Eveson and R. A. Cawson, "Warthin's tumor (cystadenolymphoma) of salivary glands: A clinicopathologic investigation of 278 cases," *Oral Surg. Oral Med. Oral Pathol.*, vol. 61, pp. 256–262, 1986.
[22] J. Lamelas, J. H. Terry, and A. E. Alfonso, "Warthin's tumor: Multicentricity and increasing incidence in women," *Amer. J. Surg.*, vol. 154, pp. 347–351, 1987.
[23] Q. Fu, F. Seier, S. K. Gayen, and R. R. Alfano, "High-average-power kilohertz-repetition-rate sub-100-fs Ti:sapphire amplifier system," *Opt. Lett.*, vol. 22, pp. 712–714, 1997.
[24] J. J. Dolne, K. M. Yoo, F. Liu, and R. R. Alfano, "IR Fourier space gate and absorption imaging through random media," *Laser Life Sci.*, vol. 6, pp. 131–141, 1994.
[25] S. K. Gayen, M. Alrubaiee, M. E. Zevallos, and R. R. Alfano, "Temporally and spectrally resolved optical imaging of normal and cancerous human breast tissues," in *Proc. Inter-Institute Workshop on In Vivo Optical Imaging at the NIH*, A. H. Gandjebakhche, Ed., Washington, DC, 2000, pp. 142–147.
[26] F. A. Marks, "Optical determination of the hemoglobin oxygenation state of breast biopsies and human breast cancer xenografts in nude mice," in *Proc. Physiological Monitoring and Early Detection Diagnostic Methods*, T. S. Mang and A. Katzir, Eds., Bellingham, WA, 1992, pp. 227–237.

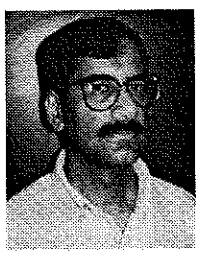

**S. K. Gayen** received the B.Sc.(Hons.) and M.Sc. degrees in physics from the University of Dacca, Bangladesh, and the Ph.D. degree in physics from the University of Connecticut, Storrs.

He is currently an Associate Professor of physics at the City College of New York and affiliated with the New York State Center for Advanced Technology for Ultrafast Photonics, City University of New York. His research interests are in optical biomedical imaging, tunable solid-state lasers, spectroscopy of impurity ions in solids, nonlinear optics, and ultrafast laser spectroscopy. He has published over 50 articles and holds three U.S. patents.

Dr. Gayen is a member of the American Physical Society and the Optical Society of America.

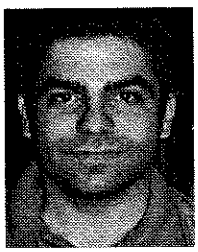

**Mohammad Alrubaiee** received his B.S. degree in electrical engineering in 1993 from the City College of the City University of New York. He is currently a graduate student in the Department of Physics and a research assistant at the Institute for Ultrafast Spectroscopy and Lasers, the City College of New York. His graduate research involves time-resolved and optical spectroscopic imaging of biomedical media.

He has published four articles in refereed journals.

**Howard E. Savage** received the B.S. and M.S. degrees from the University of Vermont, Burlington, and the Ph.D. degree in microbiology from Rutgers University, New Brunswick, NJ.

He received his postdoctoral training at Baylor College of Medicine, Waco, TX, and joined the faculty as and Instructor in the Division of Oncology, Department of Pharmacology. He was Research Associate with the Department of Head and Neck Surgery, M.D. Anderson Cancer Center, University of Texas, Austin. He joined the Head and Neck Research Service, Department of Surgery at Memorial Sloan-Kettering Cancer Center, New York, as Attending Cell Biologist and Memorial Hospital, New York, as an Assistant Laboratory Member. Currently, he has three affiliations: the New York Medical College as an Assistant Professor, The New York Eye and Ear Infirmary, Department of Pathology, as a Cell Biologist, and The Strang Cancer Prevention Clinic, New York, as an adjunct Research Scientist. Among his research interests are the use of optics to detect and follow molecular transitions in human cells and tissue.

**Stimson P. Schantz** graduated from the College of Medicine, University of Cincinnati, Cincinnati, OH, in 1975.

He is a Professor of Otolaryngology and Head, Division of Head and Neck Surgery, New York Medical College, and Head of the Department of Otolaryngology/Head and Neck Surgery, New York Eye and Ear Infirmary, New York. He is actively involved in both laboratory and clinical research and received numerous grants for conducting research on the biology and treatment of head and neck cancer. His current research interests are in the areas of genetic susceptibility, novel screening strategies, chemoprevention and biologic therapy for head and neck cancer, as well as, laser imaging in cancer diagnostics. He has published over 150 articles in peer-reviewed journals and textbooks.

Dr. Schantz is a member, and has served as director of many prestigious societies and committees. Most recently, in collaboration with international colleagues, he has founded the International Institute for Head and Neck Cancer and Tobacco-Related Diseases. He has received many honors and awards during his career, the most recent being the Harris F. Mosher Award for outstanding clinical research from the Triologic Society in 1997.

**R. R. Alfano** (M'87–SM'89–F'01) is a Distinguished Professor of Science and Engineering with the City College of the City University of New York, and Director of the Institute for Ultrafast Spectroscopy and Lasers, the New York State Center for Advanced Technology for Ultrafast Photonics, and the Center for Laser Imaging and Cancer Diagnostics, a Department of Energy Center of Excellence at the City College of New York. His research has encompassed a wide variety of areas including optical biomedical imaging, photon propagation through turbid media, ultrafast laser science and technology, ultrafast supercontinuum generation, tunable solid-state lasers, nonlinear optics, as well as dynamical processes in semiconductors, dielectric crystals, molecular systems, polymers, and biological systems. He has published over 600 papers, edited four books on ultrafast laser science and applications, organized several major conferences, and holds 81 patents.

Dr. Alfano is a fellow of the American Physical Society and the Optical Society of America.